High speed high precision ablation from ms to fs

Reinhart Poprawe [*] [a,b], Arnold Gillner [a], Dieter Hoffmann [a], Jens Gottmann [b], Welf Wawers [a], Wolfgang Schulz [†] [a,c]

[a]Fraunhofer Institute of Laser technology ILT, Aachen, Germany;
[b]Chair for Laser Technology LLT, RWTH Aachen, Germany;
[c]Nonlinear Dynamics in Laser Processing NLD, RWTH Aachen, Germany

ABSTRACT

In recent years new generations of precision lasers have been demonstrated and are increasingly available on an industrial level. For example high beam quality and diffraction limited Fiber lasers, Slab lasers, Disk lasers and still Rod lasers are used very successfully.

This paper focusses on – ns and μs drilling of shaped holes by helical drilling [1] – drilling of extreme aspect ratios in dielectrics/glass by ns-slab lasers [2] – nm-size periodic structuring of polymers by interferometric approaches – ablation by ns- and ps-pulses for metal moulds – generation of waveguide structures in glass by fs-pulses.[3] On the laboratory scale a next generation of diffraction limited short pulse lasers is at the horizon. [4] Inparticular, ps-lasers at multi-hundred watts of average power with repetition rates of several MHz,[2] fs-lasers at $400W$[2] average power and green, frequency doubled lasers at $200W$ are under construction. At the short end of pulses, attosecond lasers have been demonstrated and themselves shall open a new domain of interaction of light and matter.[5]

Keywords: laser drilling, ablation, modelling, simulation, structuring, waveguides, helical drilling

1. INTRODUCTION

The state of the art in short pulse high power laser development is summarized in Fig. 1. The upper right part of the graph is the goal for future high precision high rate ablation applications. Nevertheless, many of the partly industrially available lasers are applied in niches today and are about to expand into new markets. The processes involved are physically correlated with the laser parameters, especially, pulse length and pulse energy. Depending on the material processed, they determine modification by phase change, ablation, evaporation or melt expulsion.

2. PRINCIPLES AND MODELLING OF DRILLING

In drilling the dynamical phenomena governing the shape of the drilled hole are identified experimentally and can be related to the processing parameters theoretically. The interest is focused on the built up of recast at the drilled wall. Advances are made by relating the borders of the processing domain to dominant phenomena like ablation at the drill base, widening of the drill by melt flow and narrowing by recast at the drill wall, shadowing the beam from the drill base, recondensation of vapor at the drill wall and absorption by the plasma (Fig. 2). After reaching a typical drilled depth recast formation sets in at the entrance of the drill (Fig. 4 f). Recast formation leads to deviations from a cylindrical and tends to narrow or to even to close the entrance. Shadowing effects and aberration of the radiation take place. The distribution of the aberrated radiation deterimes the hole shape.

Mathematical model reduction using the existance of an inertial manifold is carried out and the corresponding long time limit of the underlying physical model is derived. [4,6–9] Experimental evidence (Fig. 3) shows that the final shape of the drill base is established during the first few microseconds, which underlines the mathematical arguments for a reduced model describing the long time limit. As consequence from the time scales (1) of the model, simulations (Fig. 6), and experiments (section 3) applying pulse durations in the range up to a few tenth of ns the drill terminates in a transient regime while the melt flow is not fully developped.

[*] reinhart.poprawe@ilt.fraunhofer.de, phone: +49 (0)241/8906-110
[†] wolfgang.schulz@ilt.fraunhofer.de, phone: +49 (0)241/8906-204

High-Power Laser Ablation VII, edited by Claude R. Phipps
Proc. of SPIE Vol. 7005, 700502, (2008) · 0277-786X/08/$18 · doi: 10.1117/12.785225

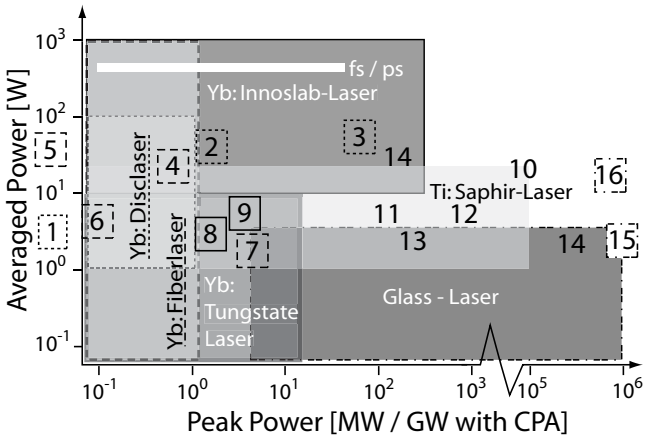

Figure 1. Laser systems and industrial availability. By Chirped Pulse Amplification (CPA) a factor 10^3 for the peak power is achievable. Yb:Disclaser (dotted): 1 Jenoptik, 2 Time-Bandwidth (without CPA), 3 TRUMPF (6.5 ps without CPA), Yb:Fiberlaser (dashed): 4 Corelase, 5 IAP FSU Jena, 6 PolarOnyx, 7 Univ. of Michigan UoM, Yb:Tungstate Laser (solid bold) 8 Amplitude Systems, 9 Light Conversion, Ti:Saphir-Laser (without borderline) 10 APRC Japan, 11 Coherent, 12 MBI Berlin, 13 Spectra Physics, 14 Thales 100/30, Glass Laser (dash-dotted) 15 Nova LLNL / Phelix GSI / Vulcan / RAP, 16 POLARIS FSU Jena, Yb:Innoslab (solid) current fs/ps-project (white bar) with specifications: $\tau_p \sim 1ps$ (Yb:YAG), $\tau_p \sim 200fs$ (Yb:KLG), $\nu_{rep} \in \{10kHz, 50MHz\}$, $P_{av} = 200W$ at $\lambda = 1030nm$.

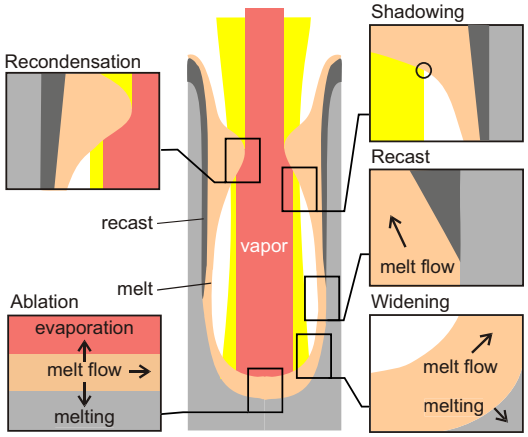

Figure 2. Ablation at the drill base, widening by melt flow and narrowing by recast at the drill wall, shadowing the beam from the drill base, and recondensation of vapor.

2.1 Initial heating and relaxation of melt flow

The time scales in the parameter range available for μs-pulses can be derived from the dynamical model. The time t_m until melting and evaporation t_v are small compared with time for relaxation t_{relax} of the melt flow. The time t_{relax} of a few μs is small compared with the time $t_\ell \simeq 100\mu s$ the flow takes for moving up the drilled depth $\ell_B = 1mm$. With the dependent quantities melt film thickness d_m, drilling velocity v_p, as well as material properties inverse Stefan-number h_m, kinematic viscosity ν, and evaporation temperature T_v, the time scales read

$$t_m = \frac{\pi}{4\kappa_s}\frac{\lambda^2(T_m - T_a)^2}{A_p^2 I_0^2}, \quad t_v = \frac{\kappa_\ell}{v_p^2}\ln\left(1 + \frac{\frac{T_v - T_m}{T_m - T_a}}{1 + h_m}\right),$$
$$t_{relax} = \frac{5}{12}\frac{d_m}{v_p}\frac{1}{1 + \frac{5}{8}\frac{\nu}{v_p w_0}}, \quad t_\ell = \frac{\ell_B}{\frac{w_0}{d_m}v_p}, \tag{1}$$

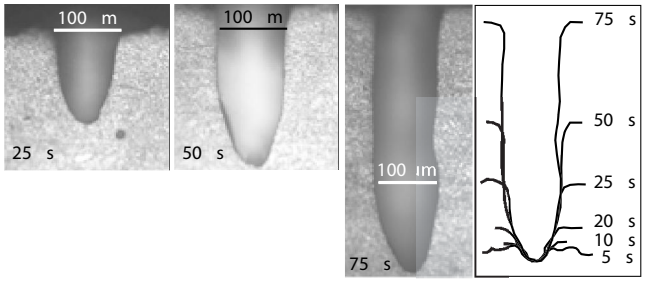

Figure 3. Shape of the single pulse drills. Cross sections for truncated pulse durations $t_{tr} \in \{5, 75\}\mu s$, (*CMSX-4*, Nd:YAG laser, $t_p = 300\mu s$, $E_p = 325mJ$)

The time t_m until melting is $t_m \approx 0.1\,\mu s$ ($T_m = 1800K$, $\kappa_s = 10^{-5}\,m^2 s^{-1}$, $A_p = 0.4$). Performing experiments with pulses truncated by a pockels cell the evolution of the drill can be observed (Fig. 4 a-c). As result, the time scales fit well to the experimental evidence.

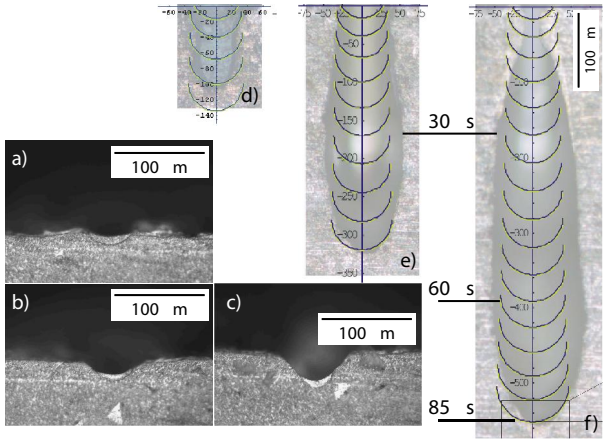

Figure 4. Cross sections of truncated single pulse drills. P ockels cell with jitter $\Delta t_p = \pm 6\mu s$. a)-c) truncated pulse duration $t_{tr} \in \{5, 10, 15\mu s\}$ (*CMSX-4*, $t_p = 300\mu s$, $E_p = 325mJ$), d)-f) Time increment $\Delta t = 5\mu s$ for simulation output. Truncated pulse duration $\{t_{tr} \in \{30, 60, 90\mu s\}$ (*X5CrNi18-10*, $t_p = 180\mu s$, $E_p = 200mJ$)

2.2 Widening of the drill by convection

There is no simple relation between the width of the laser beam and the drill, actually depending on material properties and the laser radiation. The integrated model, which covers evaporation at the drill base and melt flow along the wall as well as recast formation, shows the widening of the drill base and gives fairly well results compared to drilling experiments (Fig. 4 d-f).

Global energy balance considertion yield the ratio $F(Pe_\ell) = P_K/P_\ell$ of convective P_K und dissipative power P_ℓ depends on the Péclet-number $Pe_\ell = (V_0\, d_m)/\kappa$ only, P_ℓ is comparable to P_K, and hence the ablated volumes per time inside and outside the w_0-environment around the beam axis are of the same order of magnitude. Energy balance and the Stefan condition at the melting front yield the widening Δr of the drill:

$$\Delta r = \left(\exp(\frac{Pe_\ell}{2}) - 1\right) \cdot w_0 \tag{2}$$

As an example, for a drilling velocity $V_0 = 6\,m/s$ and a laser beam radius $w_0 = 20\,\mu m$ the widening $\Delta r \approx 0.82\,w_0 = 16\,\mu m$ of the drill corresponds fairly well to the experimental evidence (Fig. 4 d)-f)). The measured values for the width are mostly above the predicted values of this model. This argues for additional causes for widening, such as recondensation of the evaporated material, plasma heating of the drill wall or beam abberation.

2.3 Narrowing of the drill by recast formation

During drilling the laser beam dominantly heats the drill base and the melt cools down while flowing upwards along the walls resulting in recast formation on the additional time scale t_{rec}. To slow down the built up of a

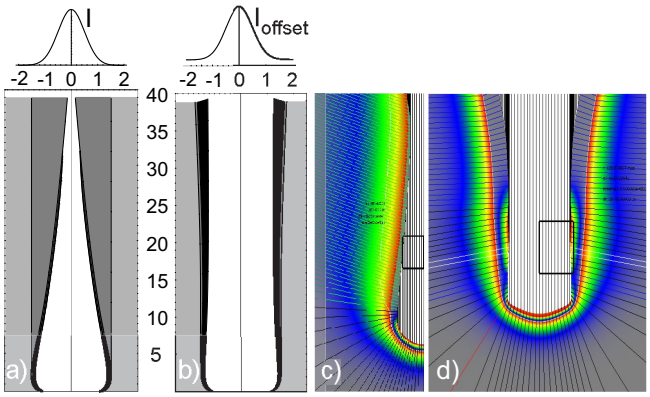

Figure 5. Simulation of the integrated model (a,b). Gaussian intensity profile without (a) and with offset (b) heating the wall: a) closure by recast (dark grey), b) heating the wall prevents recast formation, melt film (black). Lengths scale $w_0 = 20\,\mu m$. Simulation of the spatially resolved model (c,d): Temperature in the solid (ambient (grey) to melting (red)) and liquid (melting (grey) to evaporation (red)) c) no shadowing, d) geometric optical shadowing.

recast layer (Fig. 5) heating at the melt film surface along the drill wall has to balance the heat release into the solid. As result, typically a power of a few hundred Watt per mm drilled depth is sufficient to avoid recast formation. The spatially resolved model reproduces the onset of recast formation on the analytical scales and its tendency to narrow the drill and even to shadow the beam from the drill base (Fig. 5 c,d).

2.4 Melt closures of the drill

Experimental observation showing resolidified droplets beneath a closure gives a hint, that starting at a critical depth L_{krit} the drill can be closed by the melt. The melt flow slows down (7) at the entrance of the drill, the melt film thickness increases (5) with distance from the drill base, and finally starts to shadow the laser beam (Fig. 5 c). The radiation heats the closure to evaporation temperature again ejecting part of the molten closure (Fig. 5 d). This so called lift-up of the melt then happens periodically and lead to pronounced changes of the drill shape. The critical depth L_{krit} at which the drill starts to be closed, is estimated from the reduced model. The melt flow is driven by pressure Π_ℓ gradient and shear stress Σ_g. The reduced model for melt flow reads:

$$Re\left(\frac{\partial m}{\partial \tau} + \frac{6}{5}\frac{\partial}{\partial \beta}\left(\frac{m^2}{h}\right)\right) = -\frac{\partial \Pi_\ell}{\partial \beta}h + \frac{3}{2}\Sigma_g - 3\frac{m}{h^2} \tag{3}$$

$$\frac{\partial h}{\partial \tau} + \frac{\partial m}{\partial \beta} = v_p(\beta, \tau) \tag{4}$$

where $m = m(\beta, \tau)$ and $h = h(\beta, \tau)$ denotes the mass flow and the melt film thickness, respectively.

The curvature $\mathcal{K}$ of the melt film surface enters the boundary condition for the pressure, when the melt flow slows down. The corresponding dimensionless group is called the Weber-number We, scaling the ratio of hydrodynamic (ρV_0^2) and capillary pressure (σK). For $We < 1$ the surface tension σ tends to form droplets and hinders separation. The pressure Π_ℓ then is

$$\Pi_\ell \;\rightarrow \Pi_\ell + We^{-1}\frac{\partial^2 h}{\partial \beta^2}, \quad We = \frac{\rho V_0^2}{\sigma K} \tag{5}$$

The resulting motion equation is known as Kuramoto-Sivashinsky equation, which describe unstable periodic orbits and the transition to turbulence of thin film flows.

For small Reynolds-numbers ($Re \to 0$) a separation of time scales of the dependent variables can be observed. From (3),(4) the slow manifold reads

$$m = \frac{\partial \Pi_\ell}{\partial \beta} \frac{h^3}{3} + \Sigma_g \frac{h^2}{2} \tag{6}$$

The dynamics of melt flow is dominated by the melt film thickness as is well known from Lubrication theory:

$$\frac{\partial h}{\partial \tau} + \frac{\partial}{\partial \beta} \left(\frac{\partial \Pi_\ell}{\partial \beta} \frac{h^3}{3} + \Sigma_g \frac{h^2}{2} \right) = v_p(\beta, \tau) \tag{7}$$

Three major phenomena decelerate the melt at the drill wall. Friction and resolidification at the wall as well as recondensation of the vapour. As result, from (3), (4) the position $L_{krit} = \beta_{krit} w_0$ at which the drill is sealed by melt

$$L_{krit} = \frac{V_0 \, w_0^2}{\nu} \frac{2}{5} m_0 (1 - \varepsilon h_0) \tag{8}$$

just depends on the inflow m_0 of mass and the melt film thickness h_0 from the drill base ($\varepsilon = d_m / w_0$). Shadowing the radiation from the drill base by large melt film thickness is also reproduced by the spatially resolved model (Fig. 5 c, d) and a pronounced feedback of shadowing onto the shape of the drill base and the acceleration of the melt is observed.

2.5 Drilling with inertial confinement

Drilling with ns-pulse duration intensities up to $I_0 = 10^{10} W cm^{-2}$ are encountered, but the molten material is not accelerated to large velocities like in drilling with μs-pulses. The famous piston model and early FEM-calculations[10] already revealed that the acceleration of the melt flow might dominate the ablation results. However, advanceded models can handle the pronounced sensitivity of the melt flow on the details of the intensity

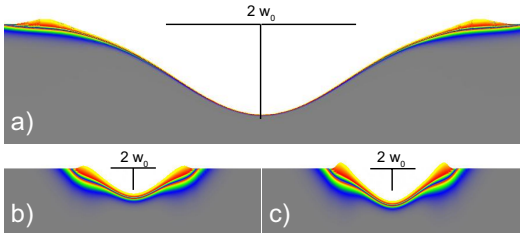

Figure 6. Simulation of single pulse drilling: The melt flow is dominated by inertia of the liquid. Most of the molten material is evaporated and the rest does not escape far away from the beam axis. For pulse durations a) $t_p = 14ns$, b) $21ns$, c) $27ns$ the melt flow is transient and widening is not yet pronounced. ($E_p = 0.5mJ$, $w_0 = 11\mu m$)

distribution (Fig. 6) and the nonlinear evaporation process. The melt flow is dominated by inertia of the liquid and does not escape far away from the laser beam axis. This behavior suggests that a moving beam can catch the recast and explains how helical drilling works with high-precision and almost no recast. During the pulse duration $t_p = 14ns$ of one single pulse in helical drilling the momentum transferred to the molten material by the recoil pressure of evaporation is too small to overcome the inertia of the melt significantly. If the drill walls reached a depth larger than the distance the melt can move, this strategy works well and almost all material is evaporated.

3. HELICAL DRILLING

To improve the precision the pulse duration can be reduced using short and ultra-short laser pulses. [11,12] Alternatively, the laser beam can be moved like in helical drilling. The effect of rotational movement is demonstrated by comparing helical and percussion drilling with identical laser parameters. To get a circular drill independent from the symmetry of the laser beam cross section, the beam movement has to consist of two synchronised

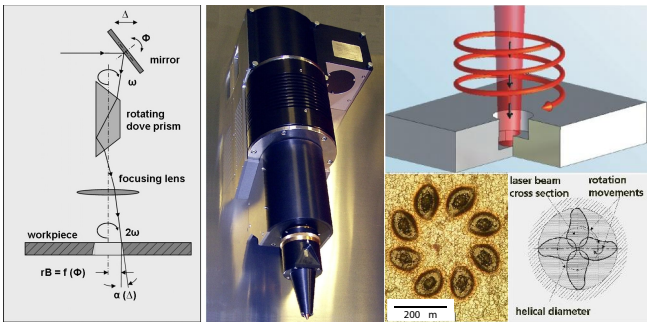

Figure 7. Helical drilling: Principle, optical setup and beam rotation movement.

rotations. One rotation moves the beam axis across the workpiece and another rotates the beam itself (Fig. 7). Like the cutting edges of a mechanical spiral bit, always the same part of the laser beam is getting in contact with the wall during one rotation. If the beam rotation is absent, the cross section of the shape of the hole reproduces the beam profile. Both rotational movements can be realised with an image rotator like the dove prism. During one cycle of the prism, the beam itself is rotated two times. If the beam is shifted parallel to the optical axis the outgoing beam axis moves on a circular path with a rotational frequency twice the frequency of the dove prism rotation. By tilting the beam with respect to the rotational axis, the outgoing beam describes a cone. The angle of the cone defines the entrance diameter and the shift results in the taper of the drill. By changing the two parameters tilt and shift, cylindrical as well as conical shaped holes with positive or negative taper are produced. If the parameters are changed during the drilling process, counterbores are also possible. The technical implementation of a helical drilling optics has been developed by Fraunhofer-ILT.[14] A dove prism is mounted into a high speed hollow shaft motor (Fig. 7). The shift of the laser beam is done by motorised movement of a laser mirror, the tilt is done by a motorised wedge prism. All motors are controlled by an external control unit, which provides an interface for changing the parameters. A half-wave-plate is also integrated into the hollow shaft motor, which rotates the polarisation synchronised to the laser beam. The drilling optics allows rotational frequencies of up to 20.000 rpm. The helical diameter has a range of 0 to 400 μm, the aspect ratio of the drillings reach up to 1:40 for 2 mm material thickness. Conical holes with an expansion ratio from entrance to exit in a range from 1:4 to 2:1 are possible. High precision helical drilling is achieved with the dove prism optics (Figure 8).

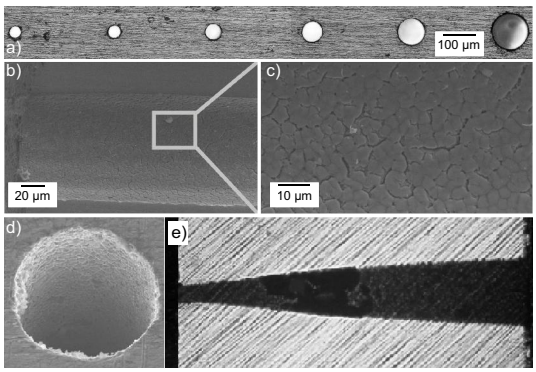

Figure 8. Results for helical drilling: a) entrance diameter from 40 to 110μm, tool steel, b) and c) hole surface in stainless steel, d) entrance diameter 80 μm, e) Cross section, entrance diameter 50μm

4. APPLICATIONS

4.1 Micro and nano structuring by laser ablation

Laser micro structuring is used for a large variety of applications in areas like electronics, automotive components, energy, sensor systems, medicine but also in the tooling industry. Today for industrial needs for fast, precise

and reproducible laser ablation single nanosecond pulses with pulse duration from $10 - 100ns$, repetition rates of $100 - 200kHz$ are used. Ablation rates of $0.1 - 1mm^3/min$ are achieved with depth accuracies of $1 - 2\mu m$.

For the ablation of thin layers and for shallow micro structuring only single overlapping pulses are used. For deep engraving and the production of three dimensional geometries like mould inserts for polymer injection moulding by laser ablation, the part geometry is generated by a three dimensional CAD-System and the data are transferred to the well known STL-Format, which is used in stereo-lithography. The area to be removed is then sliced into planes of thicknesses between $1 - 5\mu m$, depending on the ablation characteristics different for material and laser system.

The quality of the laser ablated area strongly depends on the laser parameters. Especially the laser pulse duration plays an extensive role in the formation of melt. At longer pulses the heat dissipates further in the material, which causes large amounts of molten material and higher surface roughness, since the process is controlled by melt flow behaviour. A laser with pulse duration of $100ns$ a surface roughness of $R_a = 2\mu m$ is achieved whereas pulse durations of $10ps$ lead to R_a-values $R_a < 1\mu m$ Fig. 9. The laser energy is absorbed by

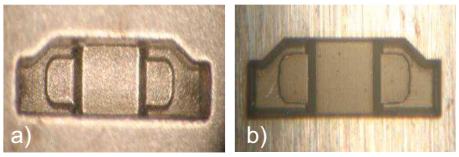

Figure 9. Laser generated micro moulding insert with pulse duration of a) $100ns$ and b) $10ps$.

the electrons and transferred to the lattice typically after a relaxation time of a few tenth ps. The short laser pulse does not interact with the produced melt and in this way the ablation takes place just by evaporation rather then by melt expulsion, which occurs after the pulse terminated. Significantly reduced ablation efficiency increased quality have to be balanced. Using pulses $\sim 10ps$, $< 10\mu J$ a layer thickness of $50 - 100nm$ can be achieved similar to classical EDM-Technologies.

In the production of micro devices, the surface properties become more important for highly loaded mechanical devices, biotechnology components and medical products with respect to wear resistance, wetting properties and chemical composition of the surface. New laser processes provide appropriate solutions for the task for applications like gliders, gears, bearings for micro mechanical devices as well as micro fluidic systems or miniaturized devices for DNA- and proteome analysis (bio-chips) and implants. With newly designed laser technologies based on nano - scale UV-laser treatment of polymers surfaces, wetting properties, cell growth behaviour and immobilization of functional molecules with high spatial resolution can modified. Functionalizing polymer and metallic part combines chemical and structural characteristics and is achieved by nano-structures with an extreme surface to volume ratio. For example, Hydrophobic/hydrophilic properties can be achieved or enhanced (i.e. laser induced lotus / anti-lotus effect, Fig. 10 b). Further examples are medical dosing equipment, where the adhesion of fluids can be avoided and thus an accurate dosage can be guaranteed with medical dosing assistance. In biological chips for medical analytics the flow characteristics and capillary effects can be functionally influenced. Enhanced roughness and chemical composition have also influence on cell growth on polymer surfaces. Thus guiding aids for cells e.g. on medical implants can be generated by laser irradiation. For direct processing different laser

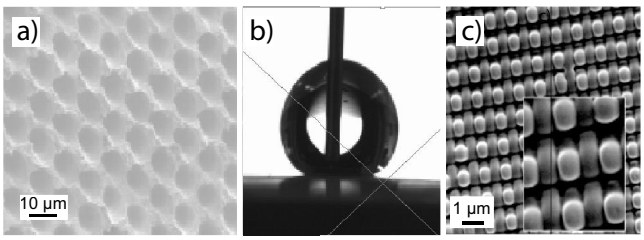

Figure 10. a) Mould surface with laser generated micro structures, b) Hydrophobic surface effect generated by micro replicated surface structures on polymer part, c) Nano structured polymer surface by UV interference irradiation

processes are available:

- Direct nano structuring of polymer surfaces by interference ablation methods
- Photochemistry based nano functionalization of polymer surfaces
- Combination of microscopic topographic change with functional surface photochemistry
- Laser based surface chemistry and molecule binding

For indirect processing the following laser processes can be used:

- Micro scale structuring of injection molding tools
- Nano structuring of tools by laser ablation of surface layers and subsequent etching

Especially the indirect methods allow low cost solutions for mass production and the equipment of consumer parts with functional nano structures and enhanced functionalities. Micro and nano structured surfaces can be combined with photochemical modifications. For the production of micro and nano-structures on three-dimensional replication tools a new laser-based process for the nano and micro structuring has been developed based on high speed scanning ablation using UV-lasers with interference imaging and direct focusing. Micro and nano scale structures in the size from $300nm$ to several μm can be produced (Fig. 10 c)

4.2 Laser supported hot embossing

A common method to enhance the formability of embossed microparts is preheating the complete workpiece. By direct heating of the tool/part with laser radiation the temperature of local regions of the work piece can be increased quickly and the achievable process limits can be extended. Transparent tool parts made of sapphire allows for direct heating within the closed tool during forming (Fig. 11). The work piece can be heated where

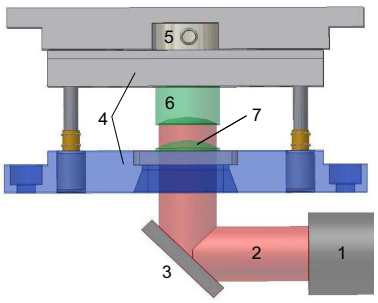

Figure 11. Principle set up of laser supported hot embossing. 1 laser optics, 2 laser beam, 3 mirror, 4 forming tool, 5 presure sensor, 6 tool insert, 7 workpiece.

the material needs to flow during forming, while other zones of the material remains cold. With this technique the forming degree can be extended and the stress of thin and sensitive tool parts is reduced.

Within laser-assisted hot embossing either the workpiece is heated up with laser radiation through a micro structured sapphire window or the forming tool is heated through the transparent workpiece. The latter approach is advantageous e.g. producing surface gratings on polymer or glass parts by micro embossing. Within several 100 ms laser irradiation the required of the forming temperature is reached and the structured punch penetrates into the workpiece. Increased accuracy and reduced embossing time are achieved by the low amount of energy is deposited in the workpiece. For embossing polymer materials are embossed in $5-10s$ and glass embossing needs $30-40s$. Micron sized dimples are embossed in polymer, which can be used as optical scattering structure (Fig. 12).

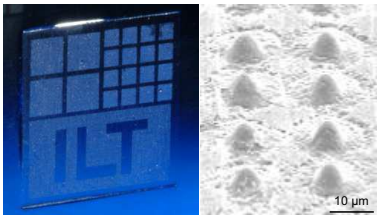

Figure 12. Hot embossed micro structures in PMMA with laser heated micro tool.

4.3 Reverse Drilling of transparent media

Laser drilling for shaping of via in transparent media has been developed. The laser beam is focussed tightly to the lower surface of the transparent workpiece, where the intense laser field initiates cracks and removes part of the material. Moving the beam in transversal direction, a well defined shape can be generated by using for instance a scanner for beam deflection. During the drilling process beam or workpiece are moved vertically. Structures with a very high aspect ratio can be generated (Example: 200:1). The diameters of via shown in Fig. 13 b) are $1mm$ and $0.4mm$. The focus diameter of the laser beam is about $10\mu m$ and allows for very precise

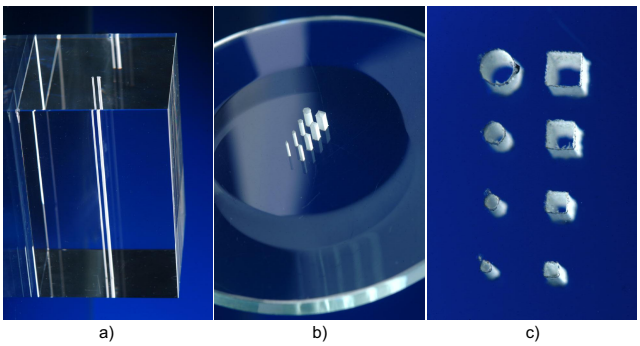

Figure 13. Laser drilled 80 mm long via in Bk7 glass a). Laser drilled via in quartz glass b) and detail c)

structuring. Figure 13 c) gives an impression of the process capabilities showing cylindrical and rectangular via with transversal dimensions from $300\mu m$ to $1000\mu m$ in quartz glass.

4.4 Structuring of waveguides by fs-laser radiation

Pulsed laser deposition (PLD) has been used in conjunction with a structuring method based on femtosecond laser ablation in order to produce laser active low loss ridge waveguides. The ridge waveguide is produced by ultrafast laser micromachining of two parallel grooves in pulsed laser deposited $Nd:Gd_3Ga_5O_{12}$ films (Fig. 14 a). The light is guided in the planar film between the two grooves and the substrate by internal total reflection.

A Yb:glass fiber chirped power amplifier (FCPA) ($\lambda = 1045nm$, $t_p = 400fs$, $\nu_{rep} = 0.1 - 5MHz$, $P_{av} = 0.4W$, μJewel D400 IMRA) and a multi pass regeneratively amplified Kerr-lens mode-locked Ti:sapphire laser (CPA Thales laser Concerto, $\lambda = 805nm$, $t_p = 100 - 3000fs$, $\nu_{rep} = 1kHz$, $P_{av} = 1.5W$) are used for the micromachining of waveguides. The femtosecond laser radiation is focused using a 63x microscope objective with $NA = 0.7$ (Thales laser Concerto) or a 50x microscope objective with $NA = 0.55$ (μJewel IMRA). The micro positioning stage (Kugler) offers an absolute accuracy of $100nm$ and a repeatability of $250nm$.

To achieve high efficiency of the laser the roughness of the waveguide edges should be less than a tenth of the wavelength, since optical losses by scattering are introduced at the rough edges or at re-deposited debris on top of the waveguide. The lateral exponential decay of the intensity is determined by detecting the scattered light with a CCD camera.

The approximation scanning method is used[27] to reduce debris formation on top of the waveguide and the extent of the heat affected zone at the waveguide edge. Using three parallel scans with $350nm$ offset results in a $1\mu m$ deep and $1\mu m$ wide groove with a smooth edge in the deposited film. Already, during the second

scan ablation takes place on the waveguide edge of the groove, the ablated material expands away from the waveguide edge reducing debris and indirect heating of the laser induced plasma. The third scan is done with a quarter of the scanning velocity to improve the precision. Using CPA laser radiation ($t_p = 100fs$) a planar wave guide structure is generated between two parallel grooves using the approximation scanning method. By writing two grooves at a scanning velocity of $40\mu m/s$ and a third groove with $10\mu m/s$, each with an offset of $350nm$ approximating the waveguide, a smooth edge of the waveguide is obtained (Fig. 14). An amorphous

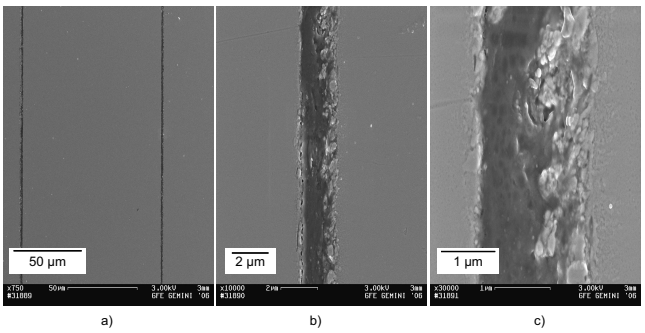

Figure 14. Ridge waveguide micro-machined by CPA laser radiation: a) Micrograph of $Nd : Gd_3Ga_5O_{12}$ ridge waveguide, b) right edge of the waveguide and c) magnification.

$Nd : Gd_3Ga_5O_{12}$ ridge waveguide laser has been successfully manufactured using pulsed laser deposition and fs-laser micro-machining[25,29] and ridge waveguides in $Er : ZBLAN$ for up-conversion application have been achieved.

A roughness $< 100nm$ of the groove is achieved by aligning the direction of polarization perpendicular to the scanning direction such that sub-wavelength ripples evolve parallel to the waveguide edge.[28] Using FCPA laser radiation ($\nu_{rep} = 100kHz$) a planar wave guiding structure is generated between two parallel grooves structured at a much faster velocity of $1mm/s$ for the first 2 grooves and $0.25mm/s$ for the last, each with an offset of $350nm$. A huge amount of debris is deposited next to the groove with a smaller amount on top of the waveguide (Figure 15a). In the groove clear sub-wavelength ripples are obtained with a period of $250 - 300nm$

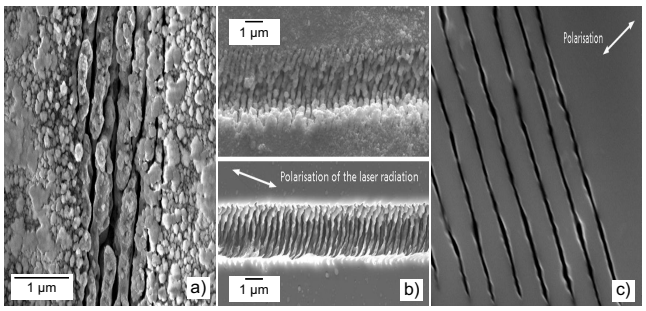

Figure 15. Microstructuring with fs-laser radiation. a) Micrograph of one groove from the $Nd : Gd_3Ga_5O_{12}$ ridge waveguide showing ripples. b) Electron micrograph of a groove structured in fused silica before (top) and after ultrasonic cleaning (bottom). ($\lambda = 1045nm$, $\nu_{rep} = 200kHz$, separation $2nm$, objective 100 x. c) Periodic nanostructures in by multiple scans with $350nm$ offset in fused silica. ($\lambda = 1045nm$, $\nu_{rep} = 250kHz$, separation $5nm$, objective 50 x.

(Figure 15a). Using a frequency of $200kHz$ and a polarization close to parallel to the scanning direction with the above approximation scanning parameters results in an increased edge roughness of the $Nd : Gd_3Ga_5O_{12}$ waveguides (Figure 15b, top). By ultrasonic cleaning the debris can be removed completely and clean periodical nano-structures are obtained (Figure 15b, bottom).

Previously demonstrated manufacturing of 2D gratings of sub-wavelength periodical nanostructures using $1kHz$ CPA laser radiation[28] is improved using FCPA laser radiation of $250kHz$ (Figure 15c). The manufacturing time is reduced by ~ 2 orders of magnitude and was only limited by the handling system.

5. SUMMARY AND OUTLOOK

To cope with the dynamical phenomena in drilling advances by combined diagnosis, modelling and simulation are presented. Using the existance of the inertial mani - fold the stucture of the solution can be analyzed to a greater detail yielding temporal and spatial scales fairly close to the numerical solution and experimental evidence. As a result, the liquid flow changes through different regimes from stagnation and laminar thin film flow at the drill base via lubrication flow at the wall to turbulent separation at the entrance. For example, percussion drilling is a strategy that miss the target of achieving a robust drilling regime while helical drilling hit the target. However, to design a robust coexistence of the strongly different hydrodynamical regimes stands to reason that fundamental research combining different disciplines offers the potential for success.

Micro and nano structuring by laser ablation today develops to tailor surface functionalization of micro mechanical devices, biotechnology components and medical products with respect to wear resistance, wetting properties and chemical composition. New laser processes provide appropriate solutions for applications like gliders, gears, bearings for micro mechanical devices as well as micro fluidic systems or miniaturized devices for DNA- and proteome analysis (bio-chips) as well as implants. Using embossing tools with nano scaled pattern, diffractive optical structures can be applied to glass and even metals at low embossing forces and short processing times.

Reverse Drilling for shaping of via in transparent media achieves cylindrical and rectangular holes with transversal dimensions from $300\mu m$ to $1000\mu m$ in quartz glass. Structuring of waveguides by fs-laser radiation demonstrates production of a ridge waveguide laser from an amorphous pulsed laser deposited $Nd:Gd_3Ga_5O_{12}$ film. The development for manufacturing waveguide lasers using fiber-CPA lasers is on the way.

6. ACKNOWLEDGEMENTS

The support of diagnosis and simulation applied to high speed drilling by the German Research Foundation under contract no. Kr 516/30-1 is gratefully acknowledged. The research related to pulse burst ablation was funded by the German Research Foundation DFG under contract no. Gi 265/4 and as part of the Cluster of Excellence "Integrative Production Technology for High-Wage Countries". Ultrafast laser micromachining was funded by Philips and IMRA supported the research with the μJewel laser in the premium application lab at LLT.

REFERENCES

[1] A. Gillner, W. Wawers, *Drilling holes*, Industrial Laser Solutions, May (2006)29-31

[2] P. Shi, K. Du, *Subsurface precision maching of glass substrate by innovative lasers*, Glass Sci. Techn., 76, 2 (2003)95-98

[3] E.W. Kreutz, A. Horn and R. Poprawe, *Electron excitation in glasses followed by time- and space-measuring tools*, Appl. Surf. Sci. 248, 1-4 (2005)66-70

[4] J. Meijer, K. Du, A. Gillner, D. Hoffmann, V.S. Kovalenko, T. Masuzawa, A. Ostendorf, R. Poprawe, W. Schulz, *Laser Machining by short and ultrashort pulses, state of the art*, Ann. CIRP, Keynote STC E (2002)531-550

[5] A. Baltuska, T. Udem, M. Uiberacker, M. Hentschel, E. Goulielmakis, Ch. Gohle, R. Holzwarth, V.S. Yakovlev, A. Scrinzi, T.W. Hansch, F. Krausz, *Attosecond control of electronic processes by intense light fields*, Nature. 2003 Feb 6, 421(6923):611-5

[6] R. Constantin, C. Foias, B.Nicolaenko, R. Temam, *Integral Manifolds and Inertial Manifolds for Dissipative Partial Differential Equations*, Springer-Verlag, New York 1989

[7] J.C. Robinson, 1995, *Finite-dimensional behavior in dissipative partial differential equations*, Chaos 5:330-345

[8] R. Poprawe, W. Schulz, *Development and application of new high-power laser beam sources*, RIKEN Review No. 50, (2003)3-10

[9] V. Kostrykin, W. Schulz, M. Nießen, J. Michel, *Short time dynamics in Laser Material Processing*, in: Nonlinear Dynamics of Productin Systems, G. Radons, R. Neugebauer (Eds.), Wiley-VCH, (2004)443-452

[10] A. Ruf, D. Breitling, P. Berger, F. Dausinger, H. Hügel, *Modeling and investigation of melt flow ejection dynamics for laser drilling with short pulses*, 3rd Int. Symp. LPM, I. Miyamoto, K.F. Kobayashi, K. Sugioka, R. Poprawe (eds.), Proc. SPIE Vol 4830(2003)73-78

[11] F. Dausinger, *Laserverfahren für Mikrobohrungen*, Springer-Verlag Berlin, Heidelberg 2000

[12] J. Kaspar, A. Luft, S. Nolte, M. Will, E. Beyer, *Laser helical drilling of silicon wafers with ns to fs pulses: Scanning electron microscopy and transmission electron microscopy characterization of drilled through-holes* , JLA, 18(2)(2006)85-92

[13] J. Radtke, *Herstellung von Präzisionsdurchbrüchen in keramischen Werkstoffen mittels repetierender Laserbearbeitung*, Herbert Utz Verlag, München 2003

[14] W. Wawers, A. Gillner, *Device for drilling and removing material using a laser beam*, patent abstract WO/2007/000194

[15] R. Stoian, M. Boyle, A. Thoss, A. Rosenfeld, G. Korn, I. V. Hertel, *Dynamic temporal pulse shaping in advanced ultrafast laser material processing*, Appl.Phys A 77(2003)265-296

[16] M. Lapczyna, K. P. Chen, P. R. Herman, H. W. Tan, R. S. Marjoribanks, *Ultra high repetition rate (133MHz) laser ablation of aluminium with 1.2-ps pulses*, Proc. 5th Int. Conf. Laser Ablation, Göttingen, Germany, (1999)883-886

[17] P. R. Hermann, A. Oettl, K. P. Chen, R. S. Marjoribanks, *Laser micromachining of transparent fused silica with 1-ps pulses and pulse trains*, Proc. Conf. Commercial and Biomedical Applications of Ultrafast Lasers, San Jose, California, (1999)148-155

[18] R. Sattmann, V. Sturm, R. Noll, *Laser-induced breakdown spectroscopy of steel samples using multiple Q-switch Nd:YAG laser pulses*, J.Phys.D:Appl.Phys. 28(1995)2181-2187

[19] S. M. Klimentov, S. V. Garnov, V. T.Kononenko, V. I. Konov, P. A. Pivovarov, F. Dausinger, *High rate deep channel ablative formation by picosecond-nanosecond combined laser pulses* , Proc. 5th Int. Conf. Laser Ablation, Göttingen, Germany, (1999)633-636

[20] C. Lehane, H. S. Kwok, *Enhanced drilling using a dual-pulse Nd:YAG laser*, Appl.Phys. A 73 (2001)45-48

[21] M. Ostermeyer, P. Kappe, R. Menzel, S. Sommer, F. Dausinger, *Laser drilling in thin materials with bursts of ns-pulses generated by stimulated Brillouin scattering (SBS)* , Appl.Phys. A 81(2005)923-927

[22] K. Walther, M. Brajdic, I. Kelbassa, *Increase of drilling velocity by use of superposed laser radiation*, Proc 4th Int. WLT-Conf. LIM, Munich, Germany, (2007)787-790

[23] K. Walther, M. Brajdic, E. W. Kreutz, *Enhanced processing speed in laser drilling of stainless steel by spatially and temporally superposed pulsed Nd:YAG laser radiation*, Int J Adv Manu Tech, (2006) DOI 10.1007/s00170-006-0768-z

[24] C. Hartmann, A. Gillner, Ü. Aydin, R. Noll, T. Fehr, C. Gehlen, R. Poprawe, *Investigation on laser micro ablation of metals using ns-multipulses*, Proc. 8th Int. Conf. Laser Ablation, Banff, Canada, (2007)440-444

[25] J. Gottmann, L. Moiseev, D. Wortmann, I. Vasilief, L. Starovoytova, D. Ganser, R. Wagner, *Laser deposition and laser structuring of laser active planar waveguides of Er:ZBLAN, Nd:YAG and Nd:GGG for integrated waveguide lasers*, Proc. SPIE. 6459, (2007)250

[26] G. Schlaghecken, J. Gottmann, E.W. Kreutz, R. Poprawe, *Pulsed laser deposition of* $Er : BaTiO_3$ *for planar waveguides*, Appl.Phys.A: Materials Science & Processing 75, (2004)1255

[27] J. Gottmann, G. Schlaghecken, R. Wagner, E. W. Kreutz, *Fabrication of erbium doped planar waveguides by pulsed laser deposition and laser micro-machining*, Proc. SPIE 4941, (2003), 148.

[28] R. Wagner, J. Gottmann, *Sub-wavelength ripple formation on various materials induced by tightly focused femtosecond laser radiation*, J. Physics: Conference Series 59(2007)333

[29] J. Gottmann, D. Wortmann, I. Vasilief, L. Moiseev, D. Ganser, *Manufacturing of* $Nd : Gd_3Ga_5O_{12}$ *ridge waveguide lasers by pulsed laser deposition and ultrafast laser micromachining* , submitted to Appl.Surf.Sci. 2007